Electron-spin-resonance linewidth of multilayered CuMn/Cu spin glasses: Residual width and thermal-broadening coefficient

D. L. Leslie-Pelecky and J. A. Cowen
Department of Physics and Astronomy and Center for Fundamental Materials Research, Michigan State University, East Lansing, Michigan 48824-1116
(Received 19 February 1993)

The electron-spin-resonance (ESR) linewidth $\Delta H(T)$ has been measured in multilayered $Cu_{1-x}Mn_x$/Cu ($x=0.07,0.11$) as a function of spin-glass layer thickness W_{SG} (1 nm $\leq W_{SG} \leq$ 1000 nm). For temperatures well above the freezing temperature T_f, $\Delta H(T)=A+BT$, where A is the residual linewidth and B the thermal-broadening coefficient. The residual linewidth increases with decreasing W_{SG}, indicating that the paramagnetic Curie-Weiss temperature Θ and/or the inhomogeneous broadening depend on W_{SG}. Preliminary high-temperature-susceptibility measurements confirm that θ decreases with decreasing W_{SG}, but are not sensitive enough to determine quantitatively if this change is entirely responsible for the observed changes in A. The thermal-broadening coefficient B characterizes the strength of the ESR bottleneck. As W_{SG} decreases, B increases, indicating the breaking of the bottleneck via the presence of additional relaxation paths. Possible mechanisms for these paths are suggested. The increase in B with decreasing W_{SG} is similar to that observed with increasing concentration of a third element in bulk spin glasses. Possible links between decreasing W_{SG} and increasing anisotropy are considered. Data parametrized in terms of ϵ, where $\epsilon=[T_f(\infty)-T_f(W_{SG})]/T_f(\infty)$, show that both A and B increase linearly with increasing ϵ over the entire range of ϵ studied.

Electron-spin resonance (ESR) is a useful technique for the study of relaxation rates in transition-ion/metallic-host systems above magnetic ordering temperatures.[1,2] The primary focus of ESR measurements above T_f in CuMn has been on the divergent behavior as T_f is approached;[3-7] however, valuable information about spin dynamics in magnetic multilayers can be obtained by analysis of the high-temperature linewidth.

We present measurements of the electron-spin-resonance linewidth $\Delta H(T)$ in multilayered $Cu_{1-x}Mn_x$/Cu ($x=0.07,0.11$) with CuMn layer thicknesses W_{SG} from 1 to 1000 nm. Section I describes the theory of the ESR linewidth in transition-ion–metal-host systems. Section II summarizes pertinent results of previous studies of multilayered spin glasses, and explains the motivation for this study. Section III contains a description of sample fabrication and measurement and is followed by the presentation and analysis of the data in Sec. IV. Section V compares our results to the behavior of the residual linewidth and the thermal-broadening coefficient in bulk Sb-doped AgMn. Conclusions are drawn in Sec. VI.

I. ESR IN TRANSITION-ION–METAL-HOST SYSTEMS

A transition-ion–metallic-host system contains three distinct components: the localized ions i, the conduction electrons of the host metal e, and the lattice L. Figure 1 shows the standard schematic picture for such a system, with arrows indicating possible relaxation paths between the components. The notation δ_{ab} represents the rate at which system a relaxes to system b.

Well above any magnetic ordering temperatures, cooperative behavior may be neglected. The Bloch-Hasegawa equations[8] of motion for the localized ions and the conduction electrons are given by Eqs. (1a) and (1b).

$$\frac{d\mathbf{M}_i}{dt}=\gamma\mathbf{M}_i\times(\mathbf{H}+\lambda\mathbf{M}_e)-(\delta_{ie}+\delta_{iL})\delta\mathbf{M}_i+\frac{g_i}{g_e}\delta_{ei}\delta\mathbf{M}_e\ , \tag{1a}$$

$$\frac{d\mathbf{M}_e}{dt}=\gamma\mathbf{M}_e\times(\mathbf{H}+\lambda\mathbf{M}_i)-(\delta_{ei}+\delta_{eL})\delta\mathbf{M}_e+\frac{g_e}{g_i}\delta_{ie}\delta\mathbf{M}_i\ , \tag{1b}$$

where $\mathbf{M}_i$ ($\mathbf{M}_e$) is the magnetization of the ions (electrons), λ is the molecular field constant, $\delta\mathbf{M}_i$ ($\delta\mathbf{M}_e$) is the change from equilibrium magnetization of the ion (electron) system, γ is the gyromagnetic ratio, and g_i (g_e) is the g factor. A detailed explanation of these equations and their solutions can be found in the review by Barnes.[1]

When the electrons can relax to the ions faster than

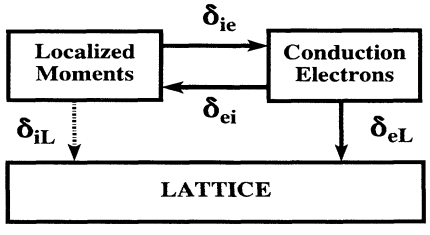

FIG. 1. Schematic diagram of localized-momentum–metallic-host systems. The relaxation rate δ_{ab} represents relaxation from system a to system b.

they can relax to the lattice, spin angular momenta transferred to the electrons from the ions can be returned immediately to the ions. Spin quanta thus become trapped between the two systems and the relaxation of the system is dominated by the bottleneck due to the slow electron-lattice relaxation rate. In the strong bottleneck limit, $\delta_{ei} \gg \delta_{eL}$ and the observed linewidth is that of the coupled spin systems. The solution of the Bloch-Hasegawa equations in the bottleneck limit is

$$\Delta H(T)=\frac{\hbar}{g\mu_B}\left[\delta_{iL}+\left[\frac{\delta_{eL}}{\delta_{eL}+\delta_{ei}}\delta_{ie}\right]\right], \tag{2}$$

where $g=g_e\approx g_i$. The first term is the residual linewidth A,

$$A=\frac{\hbar}{g\mu_B}\delta_{iL}\ . \tag{3}$$

Although Eq. (3) indicates that the residual linewidth measures the ion-lattice relaxation rate, the δ_{iL} term was added phenomenologically by Hasegawa to account for the observed temperature-independent linewidth.[1,8] This term should be interpreted as representing an inhomogeneous broadening and not necessarily as a true relaxation rate.

In the strong bottleneck limit, the second term becomes

$$\frac{\hbar}{g\mu_B}\left[\frac{\delta_{eL}}{\delta_{eL}+\delta_{ei}}\delta_{ie}\right]\approx\frac{\hbar}{g\mu_B}\left[\frac{\delta_{ie}}{\delta_{ei}}\delta_{eL}\right]\ . \tag{4}$$

The ratio δ_{ie}/δ_{ei} can be calculated[1]

$$\frac{\hbar}{g\mu_B}\left[\delta_{eL}\frac{\delta_{ie}}{\delta_{ei}}\right]=\frac{\delta_{eL}}{x}\frac{k_B m k_F}{2S(S+1)g\mu_B\hbar\pi^2}T=BT\ , \tag{5}$$

where x is the concentration of transition ions, m is the effective mass of the electron, k_B is Boltzmann's constant, S is the spin of the localized ion, and k_F is the Fermi wave number. The temperature prefactor B is called the thermal-broadening coefficient and primarily reflects the behavior of δ_{eL}. In the bottleneck limit, the thermal broadening is proportional to $1/x$. Well above T_f, the linewidth is thus linear in temperature:

$$\Delta H=A+BT\ . \tag{6}$$

In ordered magnets, as T_f is approached, the linear behavior is combined with a power-law divergence in the reduced temperature, $t=(T-T_f)/T_f$, so that the ESR linewidth for all temperatures is given by

$$\Delta H(T)=A+BT+C\left[\frac{T-T_f}{T_f}\right]^{-\kappa}, \tag{7}$$

where C is the divergence strength and κ is a critical exponent. The critical behavior of CuMn/Cu multilayers has been discussed elsewhere[9] and this paper focuses on the linear portion.

II. PERTINENT RESULTS OF PREVIOUS MULTILAYERED SPIN-GLASS STUDIES

Multilayered spin glasses have been extensively studied due to the presence of finite-size and dimensionality effects on the freezing temperature starting at the nanometer and tens of nanometers scales. Static[10,11] and frequency-dependent[12,13] susceptibility measurements of multilayered spin glasses have shown that the freezing temperature $T_f(W_{SG})$ is depressed as W_{SG} decreases. The reduced freezing temperature ϵ is given by

$$\epsilon=\frac{T_f(\infty)-T_f(W_{SG})}{T_f(\infty)}\ , \tag{8}$$

where $T_f(\infty)$ is the freezing temperature of the bulk. Standard finite-size scaling theory predicts

$$\epsilon\propto W_{SG}^{-1/\nu}\ . \tag{9}$$

Multilayers with $W_{SG}>20$ nm confirm this prediction,[11] with $\nu=1.1\pm0.1$ for all concentrations of CuMn/Cu and $T_f(W_{SG})$ extrapolating to zero at $W_{SG}\approx3$ nm. Experimental measurements, however, show that $T_f(W_{SG})$ remains finite at even a single monolayer thickness.[14] At some W_{SG} on the order of tens of nanometers, finite-size scaling fails and the continued depression of $T_f(W_{SG})$ in these samples is interpreted in terms of a crossover from three to two dimensions, as shown within a droplet model.[15–17]

Quasistatic susceptibility measurements have been made at fields up to 55 kG at a measuring frequency of about 10^{-2} Hz. Frequency-dependent susceptibility and magnetization measurements span the range from 10^{-4} to 10^4 Hz and are made at low (10^{-2} kG) fields. The ESR linewidth probes a much different part of field-frequency space ($\omega\sim10^{10}$ Hz and $H\sim3$ kG) than available with susceptibility or magnetization measurements.

Above T_f, the ESR linewidth provides two different types of information. The linear part of the linewidth probes relaxation between spin systems, as discussed in Sec. I, while the divergence is the result of the onset of spin-glass ordering. Our motivation in performing this experiment was to determine if the dimensionality crossover and finite-size effects observed in the susceptibility measurements were evident in $\Delta H(T)$. We have shown[9] that a crossover from three-dimensional to two-dimensional behavior is observed in the critical part of $\Delta H(T)$. This paper explores the changes in the linear part of the ESR linewidth as W_{SG} decreases.

III. SAMPLE FABRICATION AND MEASUREMENT

Samples were fabricated by UHV dc sputtering onto silicon ⟨111⟩ or ⟨110⟩ oriented substrates. CuMn targets were made by alloying appropriate amounts of the elemental constituents in an rf furnace. The target concentration was determined by comparing the temperature of the zero-field-cooled susceptibility cusp with known values. Alternating spin-glass layers of thickness W_{SG} (1 nm $\leq W_{SG} \leq$ 1000 nm) with 30-nm buffer layers of Cu prevents magnetic interactions between spins in different

spin-glass layers. $T_f(W_{SG})$ was determined from superconducting quantum interference device susceptibility measurements at 0.1 kG with a measuring time of about 300 sec per point. Films were removed from their substrates and mounted on flattened quartz rods with Apeizon "N" grease for measurement in a Varian 4500 spectrometer at 9 GHz.

One inherent problem of ESR in metals is the distortion of the line shape from Lorentzian to Dysonian[18] as a result of the skin depth effect. The high conductivity and resulting large attenuation of microwaves in Cu enhances this effect in CuMn/Cu multilayers. To avoid Dysonian line shapes, the total sample thickness was limited to 500–700 nm, which is approximately $\frac{3}{4}$ of the skin depth. This limitation was imposed to eliminate the possibility that changes observed in the line shape were due to the skin depth effect.

First derivative line shapes were collected by computer as the temperature was lowered from 300 K to near $T_f(W_{SG})$ and fit to a sum of real and imaginary parts of the susceptibility.[19] The ratio of real to imaginary part was held constant for all temperatures and layer thicknesses. Residual impurities from the substrate gave rise to a linear background that was accounted for in the fitting procedure.

IV. DATA AND ANALYSIS

A. Concentration dependence

Figure 2 shows $\Delta H(T)$ for "bulk" samples with concentrations of 4, 7, 11 and 16 %. Bulk here means only that no depression in T_f is observed: Both multilayers and films with $W_{SG} \geq 500$ nm are considered bulk. We note the following qualitative trends: (1) The behavior predicted by Eq. (7) is followed for all concentrations, (2) The value of the minimum linewidth increases with concentration, as is also seen in bulk $Ag_{1-x}Mn_x$,[20] and (3) The temperature at which the minimum linewidth occurs is approximately 2.5 T_f for all concentrations.

Because our desire to avoid Dysonian line shapes limits the total sample thickness, the signal-to-noise ratio for concentrations on the order of 4% was too small for accurate measurement. As W_{SG} decreases, the signal-to-noise ratio worsens, placing a lower limit on the concentration range measurable while ensuring Lorentzian line shapes. The linewidths of the $Cu_{0.84}Mn_{0.16}$ sample were very large, which made accurate extraction of $\Delta H(T)$ difficult and the fit to Eq. (7) suspect; however, susceptibility measurements of $T_f(W_{SG})$ in these samples show no anomalies and may be scaled with concentration to coincide with data from lower concentrations.[11] The analysis of W_{SG} dependence thus focuses on the 7 and 11 % concentrations.

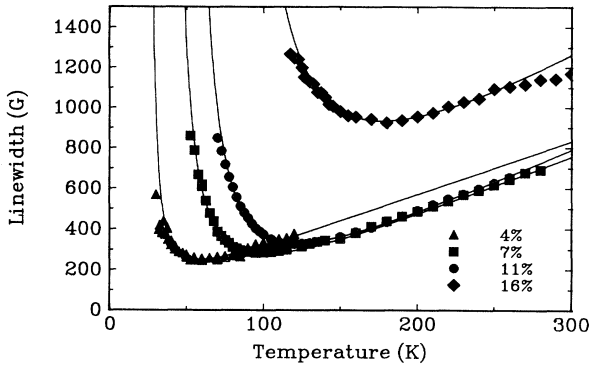

FIG. 2. Concentration dependence of $\Delta H(T)$ for 4% (triangles), 7% (squares), 11% (circles), and 16% (diamonds). Sample configurations are provided in Table I.

Table I shows the concentration dependence of the parameters in Eq. (7) for bulk samples. Excluding the 16% data, the residual linewidth decreases linearly with increasing Mn concentration at a rate of 40 G/at. %, with a residual linewidth of 0 at about 5 at. %. The significance of negative values of A will be discussed in Sec. IV B 1. In contrast to the prediction of Eq. (5), the thermal broadening *increases* slightly at a rate of 0.1 G/K at. % as the concentration increases. When δ_{eL} is primarily due to impurity scattering (i.e., δ_{eL} is dominated by terms proportional to x), B will be concentration independent. This behavior will be discussed further in Sec. VI. We briefly note that the divergence coefficient C increases with increasing concentration and that the exponent κ is 1.4±0.1 for all concentrations.

Mozurkewich *et al.*[20] studied $Ag_{1-x}Mn_x$ for Mn concentrations up to 10.3 at. %. They found that the thermal-broadening coefficient was approximately constant with x, increasing linearly at a rate of 0.03 G/K at. %. This behavior is interpreted as being consistent with the expected concentration independence of B due to the dominance of impurity scattering for concentrations greater than 1 at. %. The residual width in AgMn was found to decrease at a rate of 13 G/at. % Mn. The concentration dependence of $\Delta H(T)$ in CuMn is thus found to be qualitatively similar to that of AgMn.

B. Layer thickness dependence

Because the dependence of T_f on W_{SG} is different in different thickness regimes, direct parametrization of

TABLE I. Sample parameters and concentration dependence obtained by fitting to $\Delta H(T) = A + BT + Ct^{-\kappa}$, with $t = [T - T_f(W_{SG})]/T_f(W_{SG})$.

W_{SG} (nm)	N	c (at. %)	T_f (K)	A (G)	B (G/K)	C (G)	κ
500	Film	4	24.0	34±15	2.65±0.15	107±14	1.5±0.1
1000	Film	7	38.8	−170±20	3.01±0.10	267±7	1.3±0.1
500	3	11	47.5	−245±15	3.36±0.10	328±13	1.5±0.1
500	3	16	67.5	−184±37	4.47±0.20	672±25	1.5±0.1

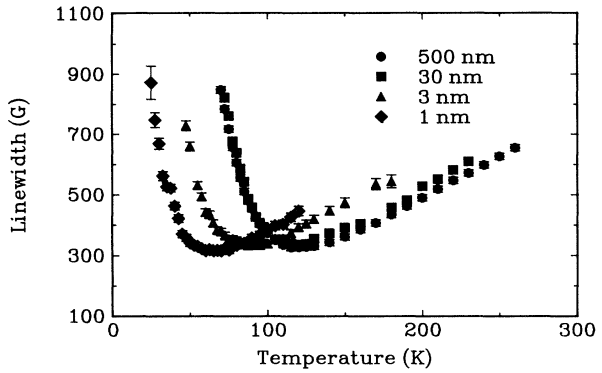

FIG. 3. Dependence of $\Delta H(T)$ on W_{SG} for $W_{SG}=500$ nm (circles), 30 nm (squares), 3 nm (triangles) and 1 nm (inverted triangles).

data in terms of W_{SG} can be opaque. Analysis of the critical behavior[9] of the ESR linewidth indicates that parametrizing the data in terms of ϵ, as given by Eq. (8), facilitates the analysis. Once the dependence on ϵ is established, either the droplet or finite-size scaling relations may be used to determine how A and B depend on W_{SG}. This parametrization also allows us to separate effects on $T_f(W_{SG})$ from effects on $\Delta H(T)$ *per se*.

Figure 3 shows $\Delta H(T)$ for $Cu_{0.89}Mn_{0.11}$ with $W_{SG}=500$, 30, 3, and 1 nm. The data are qualitatively similar, with the minimum linewidth approximately constant for all layer thicknesses; however, the position of the minimum linewidth changes from 2.4 $T_f(W_{SG})$ in the thick samples to 6.5 $T_f(W_{SG})$ in the 1-nm sample. Data for all W_{SG} (1 nm $\leq W_{SG} \leq$ 500 nm) can be fit to Eq. (7) and the results from these fits are shown in Table II. The behavior of the $Cu_{0.93}Mn_{0.07}$ series is similar, with parameters for the fit to Eq. (7) shown in Table III. The errors on the 7% data are larger, due to the weaker signal which leads to difficulty in accurately determining linewidths at high temperatures.

Frequency-dependent susceptibility measurements[12] indicate that samples with $W_{SG} \lesssim 5$ nm are better described by two-dimensional (2D) expressions. For the ESR linewidth, the 2D expression is obtained by replacing the reduced temperature t in Eq. (7) with the absolute temperature T. The exponents obtained by fitting to the 2D forms are shown in parentheses in Tables III and IV. Fitting to the 2D form does not change the values characterizing the linear portion of the linewidth.

1. *The residual linewidth*

Tables II and III indicate that the residual linewidths are negative for all W_{SG} and become less negative as W_{SG} decreases. As mentioned in Sec. I, the residual linewidth should be interpreted as an inhomogeneous broadening term and not a true relaxation rate; this interpretation requires an explanation of the significance of negative values of A.

The negative residual linewidth was explained by Stewart,[21] who pointed out that the true residual linewidth A_0 is related to the observed residual linewidth by

$$A = A_0 - B\Theta \ , \tag{10}$$

where Θ is the paramagnetic Curie-Weiss temperature and B is the thermal-broadening coefficient. When Θ is large and positive (as for the concentrations studied here), A may be negative. Tables II and III indicate that the residual linewidth becomes less negative as W_{SG} decreases. This indicates that Θ and/or δ_{iL} depend on W_{SG}.

The dependence of B on W_{SG} will be discussed in Sec. IV B 2. The other measurable quantity in Eq. (10) is the paramagnetic Curie-Weiss temperature Θ, which can be obtained from high-temperature-susceptibility measurements. As the targets used to sputter the original ESR samples had been exhausted, a series of samples with large numbers of bilayers to increase the signal size at high temperatures was fabricated from a $Cu_{0.87}Mn_{0.13}$ target. The use of a different concentration target complicates quantitative comparison with the ESR data. All susceptibility data were taken during field cooling from 400 K in the measuring field of 100 G. The two thickest samples obeyed a Curie-Weiss law, but as W_{SG} decreases, a temperature-independent background[22] becomes significant and must be subtracted from the measurements. Figure 4(a) shows the inverse of the temperature-

TABLE II. Parameters obtained by fitting $\Delta H(T)=A+BT+Ct^{-\kappa}$, with $t=[T-T_f(W_{SG})]/T_f(W_{SG})$ for $Cu_{0.89}Mn_{0.11}$. Values shown in parentheses for κ are from fits to the corresponding $T_f=0$ form.

N	W_{SG} (nm)	T_f (K)	A (G)	B (G/K)	C (G)	κ
3	500	47.5	−245±15	3.36±0.04	328±13	1.5±0.1
5	100	47.5	−245±14	3.46±0.04	324±17	1.5±0.1
6	50	45.0	−234±14	3.47±0.06	364±16	1.6±0.1
15	30	42.5	−223±14	3.51±0.06	446±16	1.8±0.1
18	10	35.0	−210±14	3.60±0.06	652±13	2.0±0.1
18	7	31.0	−198±18	3.74±0.07	896±17	2.15±0.1
18	3	20.5	−120±19	3.80±0.09	1182±21	1.7(2.55)
18	1	10.5	−70±21	4.17±0.12	2745±63	1.78(2.50)

TABLE III. Parameters obtained by fitting $\Delta H(T)=A+BT+Ct^{-\kappa}$, with $t=[T-T_f(W_{SG})]/T_f(W_{SG})$ for $Cu_{0.93}Mn_{0.07}$. Values shown in parentheses for κ are from fits to the corresponding $T_f=0$ form.

N	W_{SG} (nm)	T_f (K)	A (G)	B (G/K)	C (G)	κ
film	1000	38.8	−174±14	3.09±0.10	267±7	1.3±0.1
9	100	38.5	−170±20	3.01±0.10	308±20	1.4±0.1
6	50	36.0	−163±40	3.05±0.10	310±27	1.65±0.2
15	30	35.0	−137±23	3.19±0.14	405±20	1.95±0.15
16	5	23.5	−100±33	3.10±0.25	1485±100	2.40±0.20
17	3	17.5	−82±44	3.62±0.30	1340±131	2.1±0.2(3.1)

dependent susceptibility, $(\chi-\chi_0)^{-1}$, as a function of temperature for samples with $W_{SG}=500$, 30, 7, and 5 nm. Figure 4(b) shows the paramagnetic Curie-Weiss temperature Θ as a function of $\log_{10}(W_{SG})$. The values extracted from fitting to $\chi=C_0+C_1/(T-\Theta)$ are shown in Table IV, along with the temperature T_{depart} at which departure from Curie-Weiss behavior first occurs. These preliminary results indicate that Θ decreases with decreasing W_{SG}. The data for $W_{SG}\geq 7$ nm can be fit to a standard finite-size scaling prediction:

$$\frac{\Theta(\infty)-\Theta(W_{SG})}{\Theta(\infty)} \propto W_{SG}^{-1/\nu} \tag{11}$$

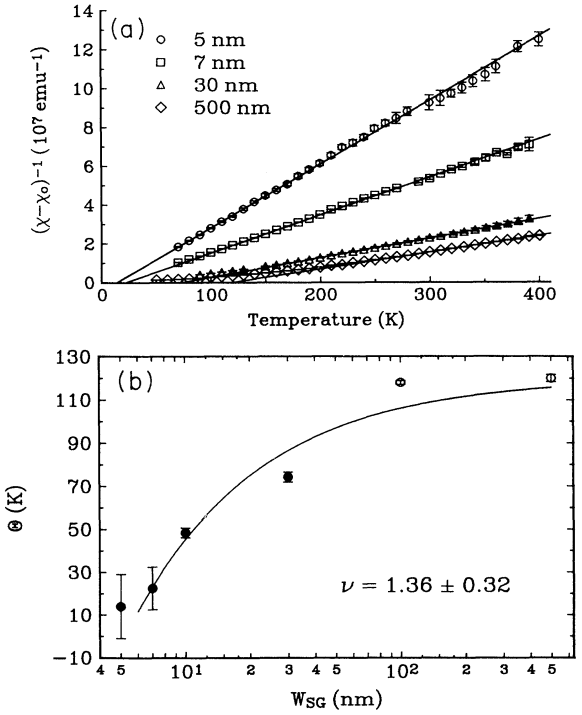

FIG. 4. (a) $(\chi-\chi_0)^{-1}$ as a function of temperature for $W_{SG}=500$, 30, 7, and 5 nm for $Cu_{0.87}Mn_{0.13}$. The solid lines represent the fits as presented in Table IV. Open symbols represent data fit with no temperature-independent background. (b) Θ as a function of $\log_{10}(W_{SG})$. The solid line represents a fit to finite-size scaling as given by Eq. (11) with $\nu=1.36\pm0.32$.

where $\Theta(\infty)$ is the bulk value of Θ. Fitting to Eq. (11) results in $\nu=1.36\pm0.32$, which is in agreement with the values found from finite-size scaling of the freezing temperature[11] and nonlinear susceptibility measurements of AgMn.[23] Further measurements are required to understand if changes in Θ are entirely responsible for the changes in A, or if A_0, which represents the real inhomogeneous broadening, is also affected by the changing spin-glass layer thickness.

As discussed in Sec. IV B 2, analyzing the ESR parameters in terms of ϵ eliminates the need to consider finite-size scaling and dimensionality-crossover regimes separately. Figure 5 shows A vs ϵ for $Cu_{0.89}Mn_{0.11}$ and $Cu_{0.93}Mn_{0.07}$ multilayers. The residual widths obey

$$A(\epsilon)=A_1+A_2\epsilon\ . \tag{12}$$

The solid lines in Fig. 5 represent the best fits to Eq. (12). For the 11% data, $A_1=-251(\pm20)$ G and $A_2=219(\pm18)$ G. The 7% data set can be fit with $A_1=-167(\pm20)$ G and $A_2=170(\pm20)$ G. Figure 6 shows $A(\epsilon)/A(\epsilon=0)$ vs ϵ. Data for both concentrations are consistent with a single line of slope 0.89 (±0.08).

The increase in the residual widths with decreasing W_{SG} is thus linear in ϵ over the entire range of ϵ considered. The relationship between the measured residual linewidth A and the true residual linewidth A_0 given by Eq. (10) explains the negative values of A and predicts that δ_{iL} and/or Θ are functions of W_{SG}. The depression of Θ with decreasing W_{SG} has been observed; further measurements are necessary to determine if the inhomogeneous broadening represented by δ_{iL} is also affected by the changing spin-glass layer thickness.

TABLE IV. Parameters obtained from fitting to $\chi=C_0+C_1/(T-\Theta)$. T_{depart} is the temperature at which the data deviate from Curie-Weiss behavior.

W_{SG} (nm)	Θ (K)	10^8C_0 (emu)	10^5C_1 (emu K)	T_{depart} (K)
500	120±2		1.16±0.01	270
100	118±1		1.18±0.06	260
30	74±4	5.34±0.10	1.00±0.04	180
10	48±3	0.60±0.04	0.413±0.01	120
7	23±10	4.12±0.13	0.511±0.05	130
5	14±15	0.82±0.02	0.306±0.05	60

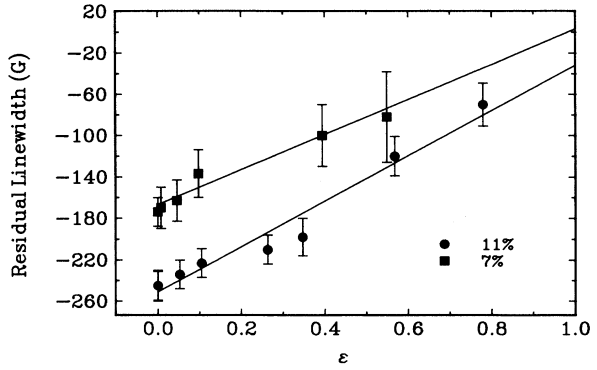

FIG. 5. The residual linewidth A as a function of ϵ for $Cu_{0.93}Mn_{0.07}$ (squares) and $Cu_{0.89}Mn_{0.11}$ (circles). Solids lines represent fits to $A(\epsilon)=A_1+A_2\epsilon$.

2. *Thermal broadening*

In contrast to the residual linewidth, the relaxation rates on which B depend represent true relaxation processes. The thermal-broadening coefficient is primarily dependent on the behavior of δ_{eL}, the electron-lattice relaxation rate. In metallic spin-glasses, δ_{eL} is due to mixing of the conduction electrons and (primarily) p states of the impurities.[24,25] The contrast between the host and impurity spin-orbit couplings produces a nonperiodic potential which results in conduction-electron spin flips. The magnitude of δ_{eL} depends on the amount of s-p mixing, the magnitude of the spin-orbit contrast, and the effect of the impurity on the local density of states.

Tables II and III show that the thermal-broadening coefficient B, which measures the strength of the bottleneck, increases with decreasing W_{SG}. As B increases, the bottleneck is "broken," as has been demonstrated in bulk CuMn and AgMn to which a third element has been added.[20,26,27] The introduction of a third element (e.g., Si, Al, etc.) provides an additional relaxation path and the pile-up of spin angular momentum between the localized ions and conduction electrons is bypassed. The behavior of B with decreasing layer thickness is similar to that seen with increasing concentrations of a third element, leading us to analyze the multilayer data using the same formalism.

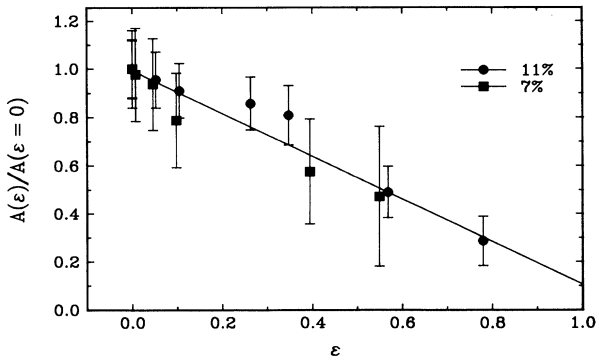

FIG. 6. The normalized residual linewidth, $A(\epsilon)/A(\epsilon=0)$, as a function of ϵ for $Cu_{0.93}Mn_{0.07}$ (squares) and $Cu_{0.89}Mn_{0.11}$ (circles). The straight line has a slope of 0.89.

When a second impurity is introduced with concentration c, δ_{eL} can be written as

$$\delta_{eL}=\delta_{eL}^{(0)}+\frac{\partial\delta_{eL}^{(1)}}{\partial x}x+\frac{\partial\delta_{eL}^{(2)}}{\partial c}c\ , \tag{13}$$

where $\delta_{eL}^{(0)}$ is the electron-lattice relaxation rate for pure copper, $\partial\delta_{eL}^{(1)}/\partial x$ is the relaxation rate per impurity (Mn) ion and $\partial\delta_{eL}^{(2)}/\partial c$ is the relaxation rate per second impurity. If we insert this relationship in Eq. (5), we find that the thermal-broadening coefficient should depend on the Mn and third-element concentrations as

$$B=\frac{\alpha}{x}+\beta+\gamma\frac{c}{x}\ , \tag{14}$$

where α, β, and γ are the appropriate constants. This analysis assumes that adding the third element does not change the density of states. In multilayers, the first two terms are due to the bulk CuMn. The last term, corresponding to the effect of the third element in bulk samples, describes the change in B due to decreasing W_{SG}. The dependence of c on W_{SG} is not obvious due to differences between the two layer-thickness regimes previously mentioned.

Further interpretation of the third term requires knowledge of the mechanisms responsible for the additional relaxation path. There are two major differences between bulk and multilayer samples: the multilayer structure (i.e., the presence of spin-glass/non-spin-glass interfaces) and the finite total thickness of the multilayer sample. The most likely mechanisms for additional relaxation in multilayers are scattering at CuMn/Cu interfaces and scattering due to the finite thickness of the samples. In CuMn/Cu multilayers, the spin-orbit contrast between Cu and CuMn layers is expected to be small compared to that between CuMn and air. Characterization indicates[11] that these samples are polycrystalline, with grains extending across spin-glass and interlayer materials, so significant CuMn/Cu interface scattering is also unlikely. Although CuMn/Cu interface effects are unlikely to be significant in this study, studies of spin-glass/insulator multilayers, such as $CuMn/Al_2O_3$, would provide an interesting test of scattering when the conduction electrons are confined to the spin-glass layers.

Scattering from free surfaces was studied by Nagashima and Abe[28] in $Cu_{1-x}Mn_x$ ($x=1$ and 5.5 at. %) films over a thickness range of 100–5000 nm. T_f should exhibit negligible change from the bulk value over this range of W_{SG}. Nagashima and Abe concluded that the probability of conduction-electron spin reorientation due to a surface collision is an order of magnitude larger than that due to collision with an impurity Mn atom; however, the effect of magnetic ordering is not included in their analysis and this may prejudice their numerical conclusions. They did not consider spin-orbit contrast as a source of additional scattering in their films. Qualitatively, they found (as did we) an increase in the residual linewidth with decreasing spin-glass thickness. The

minimum value of the linewidth in their samples increased by about 100 G as the film thickness decreased from 1230 to 250 nm (for samples of the same concentration). In contrast, we find that the minimum linewidth in our multilayers is approximately constant (for a given concentration) for all layer thicknesses from 1 to 1000 nm. This difference may be due to the sample fabrication techniques. Their samples were evaporated at a rate of several tens of nm/sec and splat cooled, while our multilayers are sputtered at a much slower rate of approximately 1–1.2 nm/sec onto substrates held between 0 and 20 °C.

If the observations of Nagashima and Abe are qualitatively correct and surface relaxation is significant at layer thicknesses as large as 1230 nm, our bulk data may already be subject to this effect. Surface scattering may contribute to the deviation of the thermal-broadening coefficient from the expected $1/x$ dependence in the bulk data of Table I. Because samples with $W_{SG} \geq 500$ nm have behaved as bulk in other measurements (i.e., no depression of T_f), ESR measurements were not made on thicker films and we have not determined if the effects seen by Nagashima and Abe are significant in these data. Further measurement is necessary to determine the physical mechanism responsible for the additional scattering paths and thus an analytic form for the last term of Eq. (14); however, further information about this term can be obtained from an analysis of the behavior of B as a function of ϵ.

Figure 7 shows $B(\epsilon)$ vs ϵ for $Cu_{0.89}Mn_{0.11}$ and $Cu_{0.93}Mn_{0.07}$. We find that the thermal broadening, like the residual linewidth, is linear in ϵ.

$$B(\epsilon)=B_1+B_2\epsilon\ , \tag{15}$$

with $B_1=4.29(\pm 0.07)$ G/K and $B_2=0.88(\pm 0.08)$ G/K for the $Cu_{0.89}Mn_{0.11}$ data and $B_1=3.03(\pm 0.15)$ G/K and $B_2=0.77(\pm 0.07)$ G/K for the $Cu_{0.93}Mn_{0.07}$ data. The 7% data show considerably more scatter, especially in the two smallest W_{SG} samples, because of the smaller signal-to-noise ratio. Figure 8 shows the normalized values of the thermal-broadening coefficients, $B(\epsilon)/B(\epsilon=0)$ for both concentrations. The data are consistent with a single line of slope $=0.25\pm 0.10$. B_1 from Eq. (15) and the $\alpha/x+\beta$ term from Eq. (14) are equivalent and describe the behavior of bulk ($\epsilon=0$) CuMn. The γ term, which includes the scattering rate per "second impurity" may be a function of x. We can equate the last terms of Eqs. (15) and (14) to find that

$$B_2(x)\epsilon(c)=\gamma(x)\frac{c}{x} \tag{16}$$

or

$$\frac{\partial\delta_{eL}^{(2)}}{\partial c}\propto\frac{x\epsilon(c)B_2(x)}{c}\ . \tag{17}$$

Because $\partial\delta_{eL}^{(2)}/\partial c$ must be independent of c, we might expect that $c\propto W_{SG}^{-1/\nu}$; however, this is valid only in the regime where finite-size scaling holds. A more general statement requires $c\propto\epsilon$, which is consistent with the result for AgMnSb (Ref. 20) discussed in Sec. V.

Determination of the form of $B_2(x)$ and of the mechanism(s) responsible for the additional relaxation path requires measurement of a wider range of film thicknesses and Mn concentrations; however, the current data indicate that the mechanism responsible for the breaking of the ESR bottleneck is a surface effect. Finite-size and dimensionality effects are seen only in the dependence of ϵ on W_{SG}, but both A and B depend linearly on ϵ over the entire range of ϵ considered. This is consistent with surface phenomena, where the surface contribution becomes increasingly significant as the ratio of surface to volume ($1/W_{SG}$) increases.

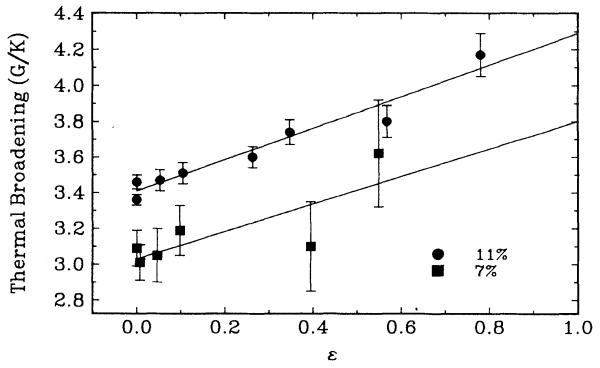

FIG. 7. The thermal-broadening coefficient B as a function of ϵ for $Cu_{0.93}Mn_{0.07}$ (squares) and $Cu_{0.89}Mn_{0.11}$ (circles). Solid lines represent fits to $B(\epsilon)=B_1+B_2\epsilon$.

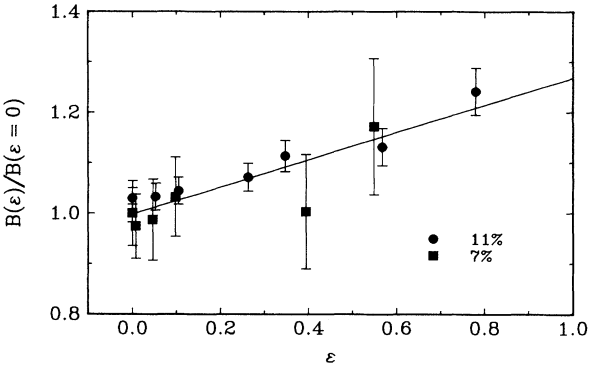

FIG. 8. The normalized thermal-broadening coefficient $B(\epsilon)/B(\epsilon=0)$, as a function of ϵ for $Cu_{0.93}Mn_{0.07}$ (squares) and $Cu_{0.89}Mn_{0.11}$ (circles). The solid line has a slope of 0.25.

V. COMPARISON TO Sb-DOPED AgMn

Analysis of the linear part of the ESR linewidth, as well as that of the divergent term, indicates similar behavior of the parameters with decreasing W_{SG} and increasing concentration of a third element. To further explore this similarity, we compare our data with the results of the study of $Ag_{1-x}Mn_xSb_c$ by Mozurkewich *et al.*[20] The original purpose of adding Sb to AgMn was to enhance the Dzyaloshinskii-Moriya anisotropy and thus test the mechanism for the linewidth divergence;

TABLE V. Comparison of fits to Eqs. (12) and (15) for $Cu_{0.89}Mn_{0.11}$, $Cu_{0.93}Mn_{0.07}$, and $Ag_{0.974}Mn_{0.026}Sb_y$.

	$Cu_{0.93}Mn_{0.07}$	$Cu_{0.89}Mn_{0.11}$	$Ag_{0.964}Mn_{0.26}Sb_y$
A_1 (G)	−167±10	−251±20	−9.5±1.7
A_2 (G)	170±20	219±18	262±21
B_1 (G/K)	3.0±0.1	3.4±0.1	2.5±0.1
B_2 (G/K)	0.77±0.30	0.88±0.08	14.9±1.0
A_2/A_1	−1.02±0.2	−0.87±0.14	−27.60±7.2
B_2/B_1	0.25±0.10	0.25±0.03	6.00±0.60

however, the freezing temperature is also reduced as the Sb concentration increases, with

$$\epsilon=[T_f(c=0)-T_f(c)]/T_f(c=0)=0.25c \ .$$

Over the concentration range studied, ϵ varies from 0 to 0.15. We can parametrize the AgMnSb data in ϵ and compare it to data from our multilayers. Note that the linear relationship between c and ϵ is inconsistent with the conclusion indicated by Eq. (17).

The residual linewidth in $Ag_{1-x}Mn_xSb_c$ increases linearly with Sb concentration at a rate of 65 G/at. % Sb for $x=2.6\%$. The data can be fit to Eq. (12), with $A_1=-9.5(\pm1.7)$ G and $A_2=262(\pm21)$ G. We are not aware of measurements that indicate if Θ varies with Sb concentration.

The thermal-broadening coefficient increases at a rate of 3.9 G/K at. % Sb at $x=2.6\%$ and can be fit to Eq. (15) with $B_1=2.5(\pm0.1)$ G/K and $B_2=14.9(\pm1.0)$ G/K. If we normalize both A and B by their bulk values and compare them to the data from Figs. 6 and 8, we find that the changes in the AgMnSb data are much more pronounced than the changes in the CuMn/Cu system for the same value of ϵ. The slope of the normalized residual width is −0.9 for the CuMn multilayers and −27.6 for the AgMn data. Similarly, the slope for the normalized thermal-broadening coefficient is 0.25 for the CuMn and 6.00 for AgMn. Table V compares the data for the CuMn and the AgMn samples. The AgMnSb data for the divergent part of the ESR linewidth can also be analyzed in terms of ϵ and follow the same dependence as in the multilayers.[29] Despite the many similarities, the limited range of ϵ considered in the AgMnSb data prevents a detailed comparison which might establish a link between increasing anisotropy and decreasing W_{SG}.

VI. CONCLUSIONS

We have measured $\Delta H(T)$ in multilayered $Cu_{1-x}Mn_x/Cu$ ($x=0.07,0.11$) spin glasses with spin-glass layer thicknesses from 1 to 1000 nm. Although $\Delta H(T)$ follows the same qualitative form for all W_{SG}, systematic changes in the parameters describing the linewidth are observed. Analysis of the data in terms of $\epsilon=[T_f(\infty)-T_f(W_{SG})]/T_f(\infty)$ eliminates complications resulting from the different dependence of T_f on W_{SG} in different spin-glass layer-thickness regimes and allows us to separate effects on $T_f(W_{SG})$ from effects on the linewidth *per se*.

The residual linewidth increases with decreasing W_{SG}, indicating that the paramagnetic Curie-Weiss temperature and/or the inhomogeneous broadening change with W_{SG}. Preliminary high-temperature-susceptibility data confirm that Θ decreases with decreasing W_{SG}, but do not exclude the possibility of changes in A_0. The residual width is found to depend linearly on ϵ for all W_{SG}.

The increase in the thermal-broadening coefficient with decreasing W_{SG} indicates that additional relaxation paths, most likely due to CuMn/air spin-orbit contrast or scattering from free CuMn surfaces, are introduced as W_{SG} decreases. Further measurements as a function of Mn concentration, W_{SG}, and interlayer material are necessary to determine the mechanisms responsible for the additional paths. Spin-orbit contrast and scattering at interfaces, while less important in CuMn/Cu multilayers, may be significant in spin-glass/insulator systems. Like the residual linewidth, B depends linearly on ϵ over the entire range of ϵ studied.

If either A or B are normalized to their respective bulk ($\epsilon=0$) values, the normalized values are consistent with concentration independence, but are not sufficient to uniquely confirm this prediction. The changes in both A and B with decreasing W_{SG} (as well as the parameters describing the divergent behavior) are similar to those observed in bulk spin glasses doped with impurities (e.g., Sb-doped AgMn). The linear dependence of A and B on ϵ is confirmed in AgMnSb, but the prefactors are much larger than those associated with the multilayers. The similarities between bulk AgMnSb and CuMn multilayers suggest the need for further investigation of the relationship between anisotropy and spin-glass layer thickness.

Finally, our results demonstrate the utility of electron-spin-resonance linewidth measurements in multilayered magnetic-ion/host-metal systems and provide a framework for their interpretation. The results presented here are not restricted to spin glasses[1] and may provide a useful compliment to resistivity measurements of multilayered superconductors[30] and other materials.[31,32] Further experimental and theoretical effort is necessary to fully utilize the potential of this technique.

ACKNOWLEDGMENTS

The authors are grateful to R. Orbach for encouraging our analysis of the linear part of the ESR linewidth and for his comments and suggestions. The authors also thank Jack Bass for helpful discussions and critical comments on this paper and M. R. Loloee for assistance with sample fabrication. The work presented in this paper was funded by Grant No. DMR8819429 from the National Science Foundation, and by the Center for Fundamental Materials Research at Michigan State University. D. L. L.-P. thanks Rockwell International for financial support.

[1]S. E. Barnes, Adv. Phys. **30**, 801 (1981).
[2]R. H. Taylor, Adv. Phys. **24**, 681 (1975).
[3]J. Owen, M. F. Brown, W. D. Knight, and C. Kittel, Phys. Rev. **102**, 1501 (1956).
[4]D. Griffiths, Proc. Phys. Soc. (London) **90**, 707 (1967).
[5]M. B. Salamon and R. M. Hermann, Phys. Rev. Lett. **41**, 1506 (1978).
[6]M. B. Salamon, Solid State Commun. **31**, 781 (1979).
[7]M. B. Salamon, J. Magn. Magn. Mater. **15-18**, 147 (1980).
[8]H. Hasegawa, Prog. Theor. Phys. **21**, 4 (1959).
[9]D. L. Leslie-Pelecky and J. A. Cowen, Phys. Rev. B **46**, 9254 (1992).
[10]G. G. Kenning, J. M. Slaughter, and J. A. Cowen, Phys. Rev. Lett. **64**, 5781 (1988).
[11]G. G. Kenning *et al.*, Phys. Rev. B **42**, 2393 (1980).
[12]P. Granberg *et al.*, J. Appl. Phys. **67**, 5252 (1990).
[13]L. Sandlund *et al.*, Phys. Rev. B **40**, 869 (1989).
[14]L. Hoines, R. Stubi, R. Loloee, J. A. Cowen, and J. Bass, Phys. Rev. Lett. **66**, 1224 (1991).
[15]Daniel S. Fisher and David A. Huse, Phys. Rev. B **36**, 8937 (1987).
[16]D. S. Fisher and D. A. Huse, Phys. Rev. B **38**, 373 (1988).
[17]D. S. Fisher and D. A. Huse, Phys. Rev. B **38**, 386 (1988).
[18]F. Dyson, Phys. Rev. **98**, 349 (1955).
[19]G. E. Pake, *Paramagnetic Resonance* (Benjamin, New York, 1962).
[20]George Mozurkewich, J. H. Elliot, M. Hardiman, and R. Orbach, Phys. Rev. B **29**, 278 (1984).
[21]A. M. Stewart, Aust. J. Phys. **33**, 1049 (1980).
[22]J. S. Kouvel and J. B. Comley, Phys. Rev. Lett. **24**, 596 (1970).
[23]L. P. Levy and A. T. Ogielski, Phys. Rev. Lett. **44**, 1538 (1986).
[24]R. Orbach, M. Peter, and D. Shateil, Arch. Des. Sci. (Geneva) **27**, 141 (1974).
[25]Y. Yafet, J. Appl. Phys. **39**, 853 (1968).
[26]A. C. Gossard, A. J. Heeger, and J. H. Wernick, J. Appl. Phys. **38**, 1251 (1967).
[27]J. A. McElroy and A. J. Heeger, Phys. Rev. Lett. **20**, 1481 (1968).
[28]Hiroyuki Nagashima and Hidetaro Abe, J. Phys. Soc. Jpn. **32**, 1507 (1972).
[29]D. L. Leslie-Pelecky and J. A. Cowen (unpublished).
[30]K. Babersschke, Z. Phys. B **24**, 53 (1976).
[31]D. A. Smith and G. P. Haberkeen, J. Phys. F **3**, 856 (1973).
[32]D. A. Smith and G. P. Haberkeen, J. Phys. F **3**, 1480 (1973).